arXiv:cond-mat/0002046v2 10 Oct 2000

Mn K-edge XANES studies of $La_{1-x}A_xMnO_3$ systems (A = Ca, Ba, Pb)

F. Bridges,[1] C. H. Booth,[2] M. Anderson,[1] G. H. Kwei,[2] J. J. Neumeier[3], J. Snyder,[4] J. Mitchell,[5] J. S. Gardner[2] and E. Brosha[2]

[1]*Physics Department, University of California, Santa Cruz, CA 95064*

[2]*Los Alamos National Laboratory, Los Alamos, NM 87545*

[3]*Physics Department, Florida Atlantic University, Boca Raton, FL 33431*

[4]*JPL, California Institute of Technology, Pasadena CA 91109-8099*

[5]*Argonne National Laboratory, Argonne, IL 60439*

Abstract

We present Mn K-edge XANES data for a number of manganite systems as a function of temperature. The main edge (1s-4p transition) for the Ca substituted samples is very sharp, almost featureless, and shifts uniformly upwards with increasing Ca content. The interpretation of this result is controversial because the lack of structure appears difficult to reconcile with a mixture of Mn^{+3} and Mn^{+4} ions. We propose a possible solution in terms of the extended Mn 4p states and hybridization between the Mn3d and O2p states. A small T-dependent feature is present in the main edge; analysis for the charge ordered (CO) sample suggests a distortion associated with the CO state that increases below T_{CO}. The manganite pre-edge structure is quite similar to that for a large number of other Mn compounds, with two or three small peaks that are ascribed to 1s-3d weakly allowed dipole transitions plus possibly a small quadrupole component. The weak dipole transitions are explained as arising from a hybridization of the extended Mn 4p state of the excited atom with an odd symmetry combination of Mn 3d states on adjacent Mn atoms. The first pre-edge peak, A_1, has a small shift to higher energy with increasing valence while the next peak, A_2, is nearly independent of dopant concentration at 300K. However, for the colossal magnetoresistance (CMR) samples the A_2 pre-edge peak shifts to a lower energy below the ferromagnetic (FM) transition temperature, T_c, resulting in a decrease in the A_2-A_1 splitting by $\sim$ 0.4 eV. This indicates a change in the higher energy 3d bands, most likely the minority spin e_g plus some change in covalency. In addition, the amplitudes are temperature dependent for the CMR materials, with the change in A_1, A_2 correlated with the change in sample magnetization. We discuss these results in terms of some of the theoretical models that have been proposed and other recent XANES studies.

PACS numbers: 75.70.Pa 61.10.Ht 71.30.+h 71.38.+i

Typeset using REVTEX

I. INTRODUCTION

The $La_{1-x}A_xMnO_{3+\delta}$ systems exhibit a wide range of different phenomena depending on the concentration, x, of the divalent substitutional atom, A (A = Ca, Ba, Sr, Pb, etc.) and the O concentration. These include ferromagnetism, antiferromagnetism, charge ordering, a metal-insulator transition, and large magnetoresistance effects. [1–6] For x roughly in the range 0.2-0.5, these systems have a ferromagnetic transition at a transition temperature, T_c, a metal/insulator transition (MI) at T=T_{MI}, and a "colossal" magnetoresistance (CMR) which reaches it's maximum at T_{MR}, with $T_{MI} \sim T_{MR} \sim T_c$ in many cases. The substitution of a divalent ion for La^{+3} formally changes the average Mn valence to 3+x (the Mn valence is +3 in $LaMnO_3$ +4 in $CaMnO_3$), and is usually thought to introduce holes into the narrow e_g band of Mn 3d-electrons, which are also hybridized with O 2p states. It is the changing occupation of this hybridized band with x that leads to many of the observed properties. Excess O in $LaMnO_{3+\delta}$ (actually Mn and La vacancies) or La vacancies can also increase the formal Mn valence, thereby adding carriers to the system.

The coupling between charge and magnetism has been modeled using the double exchange (DE) mechanism [7–9] plus strong electron-phonon coupling. [10–12] In the ferromagnetic metallic (FM) state, well below T_c, the charge carriers are assumed to be highly delocalized (large polarons) and spread out over several unit cells for CMR samples.

In the paramagnetic (PM) state above T_c for CMR samples, there is a significant increase in the distortions about the Mn atoms compared to the low temperature data. [13–17] It is generally assumed that this distortion is a result of the charge carriers becoming localized on the Mn atoms. However, mobile holes could also be located more on the O atoms as is the case for cuprates. [18] Consequently, there might be very little change in the charge localized on the Mn atoms above and below T_c. This raises the question as to how the energy shift of the absorption edge relates to valence and the local environment in these materials. Is there a mixture of "ionic-like" +3 and +4 states, an average valence, as in a metal where all Mn atoms are equivalent, or something in between?

Experimentally [15,16], the Mn K-edge absorption for the Ca substituted manganites is sharp with relatively little structure, and shifts almost uniformly with dopant concentration, consistent with an average valence state of v = 3+x. The sharpness of the edge is suggestive of a transition into a state that is uniform throughout the sample, and initially we interpreted this result to mean that all Mn sites have comparable local charge densities. This is difficult to reconcile with the usual assumption of a mixture of purely *local* ionic Mn^{+3} and Mn^{+4} sites. For example, below we show explicitly that the observed K-edge cannot be modeled as a weighted sum of the edges of the end compounds $LaMnO_3$ and $CaMnO_3$ for the charge ordered (CO) material with 65% Ca. Note however that even with similar charge densities, the d-electron wavefunctions and the local environment need not be identical at each site [19,20]. In addition, Tyson *et al.* [21] have investigated the K_β emission which probes Mn 3d states through the 3p-1s decay, and report that these spectra for the substituted manganite materials can be modeled as a weighted sum of the end compounds although the shifts with valence are small.

The pre-edge structure for the Mn K-edge consists of 2-3 small peaks labeled A_1-A_3 which have Mn 3d character. These features are observed for all the transition metals and are generally ascribed to mixture of 1s-3d quadrupole and 1s-p dipole transitions (made weakly

allowed by a hybridization between 3d states and p-states). Although the latter are assumed to be dominant, the interpretation of the A_i peaks is still controversial [22]. Two important issues are: 1) How large is the quadrupole contribution and when is it important? and 2) How are the dipole transitions made allowed since in many instances, the local environment has inversion symmetry, and in that case [23], the transition is symmetry forbidden? There have been a large number of papers in the last five years addressing these issues for many of the transition metals, not all of which are in agreement. However some questions have been answered. Since quadrupole-allowed pre-edge features have a strong angular dependence, in contrast to the dipole-allowed transitions, measurements on single crystals, as a function of angle can separate the two contributions. Such studies have shown that quadrupole transitions contribute to the A_i peaks in Ti, [22,24] V, [25,26] Ni, [27] and Fe, [27] with the largest contribution at the lowest energies of the pre-edge. The amplitude can be as large as $\sim 4\%$ of the absorption edge height for some systems at optimum orientations; but more generally it is of order 1%, and could be smaller in powdered samples which are orientational averages. The dipole-allowed A_i peaks are often in the 5-15% range and often do dominate, but not always. For example, for Ti in rutile (TiO_2), the small A_1 peak appears to be primarily a quadrupole feature. [22]

Early Mn XANES work [23,28] assumed that the A_1-A_2 splitting is produced by the crystal field parameter, often called the 10Dq parameter, which splits the t_{2g} and e_g states. These investigations did not consider the possibility of a large on-site Coulomb term, U. Recent work, using the Local Spin Density Approximation (LSDA or sometimes LDA) with and without U, and including the Hund's rule exchange parameter, J_H, find a Coulomb splitting of both the t_{2g} and e_g states, with the e_g states further split by the Jahn-Teller (J-T)interaction. [29]

Pickett *et al*, [30] (LSDA model) suggest that these systems are half metallic, with a gap between the O band and a minority spin d-band. They also point out that near 25 % Ca, all Mn sites could be essentially identical if the Ca were uniformly distributed such that there are two Ca and six La second neighbors to each Mn. Thus for the concentration range 20-30%, the local environment for each Mn may be very similar. Anisimov *et al.* and Mizokawa *et al.* [19,20] suggest that a large fraction of the d-electrons are found on the Mn atoms rather than being transferred to the O atom as in an ionic solid (thereby leaving holes in the O band). These calculations yield nearly the same electron density on each Mn atom, for sites associated with formal Mn^{+3} and Mn^{+4} valences. Other recent papers [31–34] have also stressed the importance of O, and the question of charge localization on the O atoms [35] or on the Mn atoms has been considered.

Some promising calculations for considering the pre-edge features are those of Elfimov *et al.* [36] These calculations indicate that in addition to U and J_H, there are appreciable higher order Coulomb terms that must be included and that strong hybridization occurs between the Mn 4p orbitals and the Mn 3d states on neighboring Mn atoms. The resulting splitting of the majority and minority e_g spin states results in a splitting of the Mn pre-edge features. We consider these calculations together with some of the new results on pre-edges in the discussion section.

In this paper we address the valence question and probe the Mn 3d bands using the near edge structure. Specifically we show there is no Mn K-edge shift (within 0.04 eV) through T_c. We also compare the main edge, which is too narrow to arise from a mixture of ionic

Mn^{+3} and Mn^{+4}, with the edge for a material, $Sr_3Mn_2O_{6.55}$, that does have a mixture of these ions. In addition, using a careful subtraction method, we show that there is indeed a small structure in the main edge that correlates with T_c for the CMR samples and with T_{CO} for the charge ordered material. The structure for CMR material is out of phase with that for the CO sample - which suggests that there is a distortion for the CO sample that increases at low T. We also note that the pre-edge structure has a temperature dependence which again correlates with T_c for CMR samples. The splitting of the pre-edge peaks decreases in the ferromagnetic phase which may indicate a change in covalency. Finally our interpretation of the XANES differs from earlier work on Mn K-edges but is consistent with recent studies of other transition metal atoms.

In Sec II we summarize the samples and experimental setup; some details were given earlier. [15] Then in Sec III, we provide a more extensive discussion of the shift of the Mn K-edge as a function of concentration and temperature. Here we also present the pre-edge results. We consider the implications of these results in Sec IV.

II. EXPERIMENTAL DETAILS

Many samples are used in this study, with the average Mn valence changed in a variety of ways:- divalent substitutions for La^{+3} and changes in the La^{+3} or O concentrations. Powder samples of $La_{1-x}A_xMnO_3$ were prepared by solid state reaction of La_2O_3, MnO_2, and a dopant compound - $CaCO_3$, PbO, BaO, for various divalent atoms, A. Ca substitutions are x=0.0, 0.12, 0.21, 0.25, 0.3, 0.65 and 1.0, and Ba and Pb are 0.33. Several firings with repeated grindings were carried out using temperatures up to 1400°C, with in some cases a final slow cool at 1°C per minute. The dc magnetization was measured using a commercial SQUID magnetometer. The end compounds, $CaMnO_3$ and $LaMnO_{3.006}$, show antiferromagnetic transitions at ∼130 and 125 K, respectively, while the x=0.65 sample showed features consistent with a charge ordered (CO) transition at 270 K and an AF transition at∼140 K. [5,6] Similar measurements on the substituted manganites indicates that they are all orthorhombic. The average Mn valence for several Ca substituted samples was also determined by titration (Sec. III A). See Refs. [14,15,37] for further details.

The $LaMnO_{3.006}$ sample was prepared by grinding stoichiometric amounts of La_2O_3 (Alfa Aesar Reacton 99.99%) and MnO_2 (Alfa Aesar Puratronic 99.999%) in an Al_2O_3 mortar and pestle under acetone until well mixed. The powder sample was formed into a 3/4" diameter pellet using uniaxially presure (1000lbs), and fired in an Al_2O_3 boat under pure oxygen for 12 hours at 1200-1250°C. Next the sample was cooled to 800°C, re-ground, re-pelletized, and refired at 1200-1250°C for an additional 24 hours. This process was repeated until a single phase, rhombohedral XRD trace was obtained. The reground powder was placed in an Al_2O_3 boat and post-annealed in UHP Ar at 1000°C for 24 hrs. The oxygen partial pressure was about 60 ppm (determined using an Ametek oxygen analyzer). The sample was then quenched to room temperature. Diffraction, titration and TGA measurements indicate this sample is essentially stoichiometric, with an oxygen content of 3.006.

Additional $LaMnO_{3+y}$ specimens with various average Mn valences were prepared at 1300 °C in air, followed by three intermediate regrindings. The original specimen was removed from the furnace at 1300 °C and has a Mn valence of 3.150. A piece of this specimen was

reacted overnight at 1000 °C and removed from the furnace, producing a sample with an average Mn valence of 3.206. A nearly stoichiometric specimen with average Mn valence of 3.063 was prepared at temperatures up to 1350 °C with 4 intermediate regrindings in flowing helium gas. Finally, the nonstoichiometric $La_{0.9}MnO_3$ specimen was prepared at temperatures of up to 1350 °C with three intermediate regrindings. It was slow-cooled in air at 1.5 °C/min to room temperature and had an average Mn valence of 3.312. For each of these samples the valence was determined by titration.

A sample that should have isolated Mn^{+3} and Mn^{+4} species is also needed for comparison purposes; such a material is $Sr_3Mn_2O_{6.55}$. [38] The two species are due to the oxygen defect structure that puts vacancies into the MnO_2 planes to form mixtures of square pyramids and octahedra. This highly insulating material can then be understood from chemical reasoning to be Mn^{+3} (square pyramids) and Mn^{+4} (octahedra). Some further justification for this assignment comes from the compound $Ca_2MnO_{3.5}$, which is all Mn^{+3} and has only square pyramids with vacancies in the MnO_2 planes; it is an ordered superstructure of the single-layer compound. [39] $Sr_3Mn_2O_{6.55}$ was synthesized by firing a stoichiometric mixture of $SrCO_3$ and MnO_2 at 1650 °C for 12 hr followed by rapid quenching into dry ice. This procedure is essential to prevent decomposition into α-Sr_2MnO_4 and $Sr_4Mn_3O_{10}$ on cooling and to prevent oxidation to $Sr_3Mn_2O_7$. The oxygen content was measured independently by iodometric titration and by thermogravimetric analysis, both techniques yielding 6.55(1) oxygen atoms per formula unit.

All XAFS data were collected at the Stanford Synchrotron Radiation Laboratory (SSRL). Most Mn K-edge data were collected on beam line 2-3 using Si(220) double monochromator crystals for all samples. Some data were collected on beam line 4-3 using Si(111) crystals, while most of the Mn K-edge data for the Ba substituted sample were collected on beam line 10-2 using Si (111). The manganite powders were reground, passed through a 400-mesh sieve, and brushed onto scotch tape. Layers of tape were stacked to obtain absorption lengths $\mu_{\rm Mn}t \sim 1$ ($\mu_{\rm Mn}$ is the Mn contribution to the absorption coefficient and t the sample thickness) for each sample. Samples were placed in an Oxford LHe flow cryostat, and temperatures were regulated to within 0.1 K. All data were collected in transmission mode. A powdered Mn metal sample was used as an energy reference for each scan. The pre-edge absorption (absorption from other excitations) was removed by fitting the data to a Victoreen formula, and a simple cubic spline (7 knots at constant intervals $\sim$140 eV in E) was used to simulate the embedded-atom absorption, μ_0, above the edge.

The edge shifts are reported relative to a Mn powdered metal foil for which we take the position of the first inflection point to be 6537.4 eV. [16] For each scan, the position of the reference edge was determined by fitting the edge to that of a fiducial scan. This provided a correction to the relative edge position consistent within $\pm$ 0.015 eV - see next section.

In the pre-edge region there is a remnant of the La L_I XAFS that must be considered; the oscillation amplitude is about 0.3 % of the Mn step height, just before the pre-edge. However, the La K-edge XAFS show that there is a "beat" in the XAFS from about 8.4-10 $Å^{-1}$, which for the La L_I XAFS corresponds to the range of the Mn XANES. In this beat region the La L_I XAFS is reduce by another factor of 4; thus the La oscillations underlying the Mn XANES region has an amplitude of about 0.08%, much smaller than the changes we investigate. In addition, this oscillation is slowly varying with energy, and would at most produce a slowly varying background. Consequently any remaining La L_I XAFS are not a

problem for the Mn XANES study.

III. NEAR EDGE RESULTS

A. Main edge

In Fig. 1 we show the Mn absorption K-edge for several concentrations of Ca, 33% Ba and Pb, $La_{0.35}Pr_{0.35}Ca_{0.3}MnO_3$, a $Sr_3Mn_2O_{6.55}$ sample that should have a nearly uniform mixture of ionic Mn^{+3} and Mn^{+4}, some O excess samples, and a La deficient sample.

For the Ca substituted samples several points are immediately obvious: (1) To first order the main absorption edges (ignoring pre-edge structures for now) have almost the same shape for each dopant concentration and shift nearly rigidly to higher energy as the concentration is increased, (2) the edges for the manganite samples are very sharp, roughly half as wide as the edge for the $Sr_3M_2nO_{6.55}$ sample, (3) there is no obvious kink or structure in the sharp edges for the substituted (La,Ca) manganite samples that would indicate a simple mixture of Mn^{+3} and Mn^{+4} ions, (4) however, there is a tiny shape change, visible in Fig. 1 for samples of different concentration, which shifts the *position* of the inflection point on the edge relative to the half height position.

The data for the $La_{0.35}Pr_{0.35}Ca_{0.3}MnO_3$ sample looks very similar to that for $La_{0.7}Ca_{0.3}MnO_3$ indicating that replacing some of the La by Pr does not change the local electronic configuration on the Mn. The O excess and La deficient samples show a similar edge shape to $LaMnO_3$, but the edge shift is considerably smaller than expected based on the Mn valence obtained from TGA. The shifts for the O excess data are inconsistent with data from other groups [40,41] and are included here to show the sharpness of the edge. However, such data suggest that the position of the Mn K-edge is determined by several factors and using the Mn valence and O content obtained from TGA may not be sufficient.

In contrast to the Ca substituted materials, Ba and Pb substitution results in a significantly broader edge, more comparable to the edges of other Mn oxides [23,42,43] and the $Sr_3Mn_2O_{6.55}$ sample. There is relatively more weight in the lower part of the edge.

In addition to the shift of the inflection point position on the edge with Ca concentration, as noted above, the region of steepest slope is also quite broad. Consequently using the position of the peak in the first derivative curve as a measure of the average edge position (as we and others have done previously) is only an approximate measure of the average edge shift. Using the derivative peak yields a roughly linear shift with concentration. [15,16,44] Our data and that of Subías *et al.* [16] have the same edge shift per valence unit, while the shift reported by Croft *et al.* [44] is smaller. This may be the result of different O content in the samples.

To obtain a better estimate of the average edge shift with concentration (at room temperature), we have fit the $LaMnO_3$ edge data (or the $CaMnO_3$ data) to that for each of the other samples, over the main part of the edge (above the pre-edge structure). In this procedure it is important that when the absorption from other atoms is removed, the data base-line below the pre-edge structure be at zero. Each edge is also normalized using some feature of the data; for the data at different concentrations, we normalized over a range of energies well above the edge, where the XAFS oscillations are small. Similarly we fit the

corresponding reference edges (Mn foil) to a reference scan to obtain a net overall edge shift. Several examples of these fits are shown in Fig. 2. Although there is a change in shape between $LaMnO_3$ and $CaMnO_3$, the relative shifts determined with either end compound are nearly identical - less than 0.02 eV difference over the entire concentration range.

In Fig. 3a we plot the relative shifts obtained from fits to $LaMnO_3$ at room temperature. The shift with x is roughly linear with concentration, with a net shift from 0 to 100% Ca of ∼3 eV. This is considerably smaller than the value 4.2 obtained from the derivative peak [15,16] and illustrates the effect of the shift of the inflection point relative to the half height. However, over the straight part of the plot from x= 0.3-1.0, the slope is 3.3 eV/valence unit, quite close to the 3.5 eV/valence unit obtained by Ressler *et al.* [45] for MnO, Mn_2O_3, and MnO_2. The point at x = 0.12 is anomalous, but titration measurements give about the same Mn valence for the 12 and 21% samples, which agrees with the comparable edge shifts. The same data is re-plotted as a function of the titrated valence in Fig. 3b; in this case the variation with valence is smoother, but slightly non-linear. The different values for the titrated valence, compared to the value expected from the Ca concentration may indicate that there are slight variations in O content in some samples.

We have also used a similar analysis to investigate any possible edge shift as a function of temperature, by fitting the entire edge of the 50K data for a given sample to all the higher temperature data files. Two examples are shown in Fig. 2c,d. This figure shows that changes in the shape of the main edge, above and below T_c, are quite small (although measurable). The largest relative change is in the pre-edge peaks, to be discussed later. In Fig. 4 we show the shift of the edge position as a function of temperature up to 320K for several sets of samples. (We have similar data out to nearly 500K for the Ba sample and $CaMnO_3$.) Variations in the fit values for the net shift, ΔE_o, for several traces at the same temperature are less than ± 0.02 eV, and fluctuations about the small average shift with T are comparable for a given experimental run. Differences between experimental set-ups or using Si<111> or Si<220> monochromators are less than 0.1 eV. For T less than 300K, the net shift for each sample is very small (less than 0.04 eV), but nearly all appear to have a slight decrease at high T.

B. Pre-edge region

In Fig. 5 we plot the pre-edge region as a function of temperature on an expanded scale for $CaMnO_3$, a CMR sample with 21% Ca, and the 33% Ba sample. Data for $LaMnO_3$, the CO sample with 65% Ca and another CMR sample have recently been published [46] in a short paper. For these systems the main features are the lower three peaks labeled A_1-A_3 (near 6539, 6541, and 6544 eV) and the B peak. The lower two peaks A_1 and A_2 are common to all materials although not resolved for the 33% Ba data collected using Si (111) crystals which have a lower energy resolution. The comparison of the two Ba data sets in this figure illustrate the importance of using high energy resolution. The A_3 peak is not obviously present in most samples. In Fig. 6 we compare the data for the 30% Ca CMR sample with the $Sr_3Mn_2O_{6.55}$ sample and also show the pre-edge for the Pb sample, all on a more expanded scale.

There are several features to note; all the pre-edge features start at very nearly the same

position regardless of doping and the amplitude of the pre-edge features labeled A increases with average Mn valence (Ca concentration) as observed in other Mn compounds [23] and in a previous manganite study. [44] There are, however, small shifts of these features with Ca concentration as shown in Fig. 7. The A_1 peak energy increases slightly from $LaMnO_3$ to $CaMnO_3$, and the A_1-A_2 splitting decreases from 2.2 to 1.8 eV. (The exception is the 65% sample, but here the A_i peaks are poorly resolved.) For the substituted samples, the leading edge of the A_1 peak remains steep for all concentrations except the 65 % sample. Consequently, the pre-edge for the intermediate concentrations (CMR samples) cannot be modeled as a simple weighted sum of the end compounds $LaMnO_3$ and $CaMnO_3$. Note that the leading edge for the $Sr_3Mn_2O_{6.55}$ sample (See Fig. 6) is broader, consistent with a mixture of Mn^{+3} and Mn^{+4} ions, and also has a significant A_3 peak. The latter is not present in the data for 30% Ca.

The Ba and Pb pre-edges are slightly different; the Ba pre-edge features are not as well resolved even for the higher energy resolution data while the A_1 peak is largest for the Pb sample (Compare Fig. 6 with Fig. 5).

The most striking feature in Figs. 5,6 is the variation in the intensity of the pre-edge peaks and the shift of A_2 as T increases through T_c for the CMR samples. In contrast, the change for $LaMnO_3$ is small up to 300K. [46] For the 21% Ca sample in Fig. 5 the A_1 peak decreases in amplitude while the A_2 and B-peaks increase with increasing T; the A_2 peak is sharpest at 300K and clearly shifts downward below T_c (0.4 - 0.5 eV, depending on the background function used). See the solid triangles in Fig. 7. The change in the A-peaks for the 33% Ba sample (using the high resolution monochromator) appear to follow the same trend as observed for the Ca data (Fig. 6) but the A_2 peak is not as well resolved.

The largest temperature dependence is observed for the $CaMnO_3$ sample above 300K (See Fig. 5a), with the largest increase occurring for the B-peak. Also, the amplitude of the peak at the top of the edge, commonly called the "white line", (see Fig 1c at 6554 eV for example) decreases slightly at high T. These effects become much larger at only slightly higher temperatures and will be treated in a separate paper. For the CMR samples, we associate the temperature dependent changes in the amplitude of the pre-edge features with changes in charge localization/hybridization.

C. Difference Spectra

More detailed information can be obtained by examining the change in the shape of the XANES region as a function of temperature. The files are first shifted to correct for any small changes in the energy of the monochromator and all spectra are carefully normalized as discussed earlier. The difference spectra are obtained by subtracting the data at 300K from all the data files (at different temperatures) for a given sample. This approach was used originally to investigate the pre-edge region for the 21% sample, [46] but considerable structure was found at energies corresponding to the main edge, for both the CMR and CO (x=0.65) samples. Several examples of these difference spectra are shown in Fig. 8 for $LaMnO_3$, $CaMnO_3$, and the 21, 30, and 65 % Ca substituted samples.

In the pre-edge region, the temperature variation of the A_1 and A_2 peaks for the 21 and 30% Ca (CMR) samples is very clearly visible in Fig. 8c,d; it begins at T_c, with most of

the change occurring over a 60K range just below T_c. The temperature-dependent changes of the pre-edge are comparable in both samples, with the magnitude of the change of the A_2 peak being roughly 50-70% that of the A_1 peak. For the 65% Ca sample, changes of the A_i with T are also observed in the different spectra, but the amplitudes are considerably smaller, and interestingly, the phase is inverted - the A_1 difference peak decreases instead of increasing. For the $LaMnO_3$ sample (Fig. 8a) there is essentially no structure in the difference spectra over the pre-edge energy range, but surprisingly there are small peaks in this range for $CaMnO_3$ (See lower part of Fig. 8a), with the largest peak in the difference spectra occurring *between* A_2 and A_3 - this suggests that there are in reality more than three pre-edge peaks.

There is also well defined structure in the difference spectra over the energy range of the main edge, although it is only a few percent of the edge in amplitude. For $LaMnO_3$ there is a broad feature over most of the edge region which increases as T is lowered. $CaMnO_3$ has a similar feature but it is larger and narrower (Fig. 8a). Both appear to correspond to the temperature dependent peak near the top of the edge (the "white line" mentioned earlier) which is sharpest at low T. For the CMR samples, there is additional structure on top of this broad peak - a dip at 6551 and a peak at 6553 eV (2 eV apart). Another dip/peak occurs just above the edge at 6555-6556.5 eV. The CO sample also shows structure over this energy range but again the phase is inverted relative to the CMR samples (i.e. a peak/dip at 6552 and6554 eV), - this phase inversion thus extends over the entire near-edge region.

IV. DISCUSSION

A. Main edge

For Mn atoms the main K-absorption edge represents transitions mainly from the atomic 1s state to the empty Mn 4p band. The XANES results show that this edge is very sharp for the Ca-substituted samples, the O-excess samples and the La deficient sample. The width of the edge (roughly 5-6 eV) is narrower than the edge for most other Mn compounds and the shift in edge position is $\sim$ 3 eV for a valence change of +1. No obvious indication of a step or double edge structure is present that would indicate two distinct valence states. If completely localized Mn^{+3} and Mn^{+4} ions were present on time scales of 10^{-14} sec, the edge should have a smaller average slope and generally be broader, as would be expected for a mixture of fine powder of $LaMnO_3$ and $CaMnO_3$. To model this explicitly, we compare in Fig. 9 the experimental edge for the 65% Ca (CO) sample and a weighted sum of the +3 and +4 end compounds; clearly the experimental edge is much sharper as noted previously. [15,16]

In contrast to the Ca-doped samples, the edge for $Sr_3Mn_2O_{6.55}$ is much broader (Fig. 1a), with a width of 10-12 eV. There is also a change of slope of the main edge for this sample that is consistent with two valence states, but the shape is more complicated. Note that a combination of two edges each $\sim$5 eV wide, separated by $\sim$3 eV (the separation for a valence change of 1) would yield an edge of width $\sim$ 13eV. Thus the width and structure of the $Sr_3Mn_2O_{6.55}$ edge are both consistent with the expectation that two valence states

are present in this sample – Mn^{+3} and Mn^{+4}. Similarly our data for Mn_3O_4, which has a mixture of +2 and +3 valence states, has a very broad edge of 13-14 eV (not shown).

The edges for the Ba and Pb samples are also broader; they have a break in slope and more amplitude in the lower part of the edge that might suggest two valence states. In this regard they are quite different from the Ca substituted samples for which the shape of the main edge for the CMR samples does not change much from that of $LaMnO_3$. In addition, the net shifts of the edges for the 33% Ba, and Pb samples are smaller than expected; the additional structure near 6546-48 eV shifts the lower part of the edge down in energy while the top of the edge is close to the position of the 30% Ca samples. The net result is a very small overall average edge-shift compared to $LaMnO_3$.

We have also shown by fitting over most of the edge, that there is no significant change in the average edge position for any of the substituted manganite samples near T_c. This agrees with our earlier result [15] in which we averaged data points above and below T_c. The new analysis also indicates that there is consistently a slight decrease in edge position at the highest temperatures, that is largest for $CaMnO_3$ and $Sr_3Mn_2O_{6.55}$. The reason for this downward shift is not yet clear but may be related to the temperature dependence of the B peak (since an increase in the B-peak intensity effectively shifts the lower section of the edge to lower energy).

However, the lack of any temperature dependence below T_c disagrees with the earlier work of Subías *et al.*, [16] who report a 0.1 eV decrease in edge position up to T_c for $La_{0.6}Y_{0.07}Ca_{0.33}MnO_3$ and then a 0.09 eV increase up to 210K. The small but important change in the shape of the main edge in Fig. 8 provides a partial explanation for this discrepancy. Subías *et al.* assumed no change in edge shape and calculated difference spectra for each temperature. Under this assumption, the amplitude of the peak in the difference spectra would be proportional to the energy shift of the edge. The additional structure observed in the difference spectra indicates there is a shape change rather than an overall edge shift.

The difference spectra (Fig. 8) also show clearly that the additional structure is dependent on T_c. For the CMR samples, the dip-peak structure, superimposed on the peak observed for the end compounds, begins to be observable near T_c and grows rapidly in the 60-100K range just below T_c. This structure means that compared to the edge at low temperatures (undistorted Mn-O bonds) the edge above T_c (distorted Mn-O bonds) has the upper part of the edge shifted upward in energy while the lower part is shifted downwards. The separation between the dip-peak structure is about 2 eV (see vertical dotted lines).

This raises several questions - for the CMR samples is there a mixture of +3 and +4 sites as usually assumed? If so why is the edge structure so small? Can the small structure observed in the difference spectra be explained in some other way? One aspect that must be included is the very large width of the Mn 4p density of states (DOS), roughly 15 eV wide, that is found in two quite different recent calculations. [36,47] The main edge is due to transitions into this band and the calculated absorption edge [36] (broadened by the core-hole lifetime) is very similar to that observed experimentally. [46] The broad width means that the 4p states are extended and not localized on one Mn atom. Consequently, the K-edge will correspond to a Mn valence partially averaged over several Mn atoms, and thus will be less sensitive to variations in local charge on different Mn sites.

Another possibility is that the system is more covalent and that there are some partial

holes in the O 2p band which is hybridized with the Mn 3d states. This is supported by several calculations and by the observation of holes in the O 2p band in absorption studies [35]. Such holes may play an important role in the unusual transport of these materials. In calculations, Anisimov *et al.* [19] and Mizokawa and Fujimori [20] obtain two types of Mn e_g configurations with almost identical local charge densities. In both calculations there are distortions of the Mn-O bond distances. For the calculation of Anisimov *et al.* [19], one configuration is symmetric in the *ab* plane with four small equal lobes directed towards O while the other has two large (and two small) lobes, again directed towards O atoms in the *ab* plane. The more symmetric case is associated with a formal Mn^{+4} site and the other state with Mn^{+3} but because the charge densities are comparable would not lead to significantly different edge shifts. The recent calculations of Elfimov *et al.* [36] are also relevant. To fit the observed splittings of A_i peaks (2.2 eV for $LaMnO_3$ and 1.8 eV for $CaMnO_3$), U and J_H had to be lowered from the values in the first calculation [36] - to 4 eV and 0.7 eV, respectively, [46] which implies higher covalency.

The remaining question to be answered about the main edge for the CMR samples is what is the explanation for the small structure in the difference spectra as T is lowered below T_c? A possible answer is again found in the calculations of Elfimov *et al.* [36]. They find that the position of the 4p partial DOS is bond-length dependent - it occurs at a lower energy when the Mn-O bond lengthens (p_x orbitals in their paper) and is at a higher energy for shorter bond lengths ((p_y and p_z). Such a shift is expected; in polarized XAFS experiments on high T_c materials we have observed edge shifts between the c- and a-axes. In addition, studies of molecules show that the edge shifts to higher energy when the bond length shortens. [48] The separation between the partial DOS for p_x and p_y is about 2 eV in Elfinov *etal*'s calculation when they use distortions similar to those observed in $LaMnO_3$; we expect to see some evidence of this splitting in the experimental absorption edge, although it is lifetime broadened and the 4p states are extended. We propose that the tiny dip-peak structure observed for the CMR materials is the result of the different positions for the partial DOS for p_x and p_y. The dip-peak splitting is also about 2 eV but it is not clear whether this is significant or a coincidence.

For the CO sample there is also structure in the edge but the phase is inverted. If the above explanation for the *dip-peak* structure in the difference spectra for CMR samples is correct then it suggests that the *peak-dip* feature for the CO sample is also produced by local distortions - but in this case by a local distortion that starts at the charge ordering temperature, T_{CO}=270K, and *increases* as T is lowered. Such a model then provides a simple interpretation for the unusual lack of temperature dependence (reported [15] but not explained) for σ^2 for this sample. The surprise is that at least the thermal phonon broadening should have caused some increase in σ^2 with T. However, if there is a distortion associated with the CO state, then there must be an associated broadening contribution σ_{CO}, for the Mn-O pair distribution function, σ^2_{CO}, that is zero above T_{CO} and increases as T is lowered below T_{CO}. Then the total variance for the Mn-O bond, σ^2_{Mn-O}, will be given by

$$\sigma^2_{Mn-O}(T) = \sigma^2_{phonon}(T) + \sigma^2_{CO}(T) + \sigma^2_{static} \quad (1)$$

where $\sigma^2_{phonon}(T)$ is the phonon contribution, and σ^2_{static} is a static (temperature-independent) contribution from disorder. $\sigma^2_{phonon}(T)$ should be comparable to that for $CaMnO_3$, since we

see the same phonon component for both pure $CaMnO_3$ and $La_{0.79}Ca_{0.21}MnO_3$ above T_c. To make σ^2_{total} nearly independent of T means $\sigma^2_{CO}(T)$ and $\sigma^2_{phonon}(T)$ almost cancel for temperatures below 300K.

We can extract the CO contribution following the method in Ref. [15] for calculating $\Delta\sigma^2$ - we fit the two highest T data points (from Ref. [15]) to $\sigma^2_{phonon}(T) + \sigma^2_{static}$ and then subtract these contributions from the data. In Fig. 10 we plot the result of this analysis for the 65% Ca sample. From this figure, the maximum value for $\sigma^2_{CO}(T)$, is roughly 10% of that associated with polaron formation for the CMR samples. Such an increased distortion for charge ordered material makes sense - as the sample becomes charge or orbital ordered, there is more room for the longer Mn-O bonds to lengthen, while for a random arrangement of orbitals, the series of long and short Mn-O bonds are more constrained.

B. Pre-edge region

1. Background

The pre-edge results provide additional information about the nature of the electronic states. For many of the transition elements, 1-3 pre-edge peaks, A_i, occur well below the main edge ($\sim$ 15eV below) and are assigned to transitions to empty states with d-like character, i.e. these are 1s to $3d^{(n+1)}$ transitions [49,50] where n is the initial number of d electrons and n+1 includes the excited electron in the final state, which usually includes the effect of a core hole. The 1s-3d transitions are directly allowed through the very weak quadrupole transition [23,22,24–27] or allowed via an admixture of 3d and 4p states [23,22,25,27,46]. In the pre-edge region there may also be some hybridization with the O 2p states. If the metal site is centrosymmetric, there is no mixing of 3d and 4p states on the excited atom and 1s-3d dipole transitions are strictly forbidden; [23] however local distortions can make such 1s-3d transitions very weakly dipole allowed. Three aspects need to be recognized in considering the Mn pre-edge in the present study.

- *Quadrupole interactions*
  Although the quadrupole interaction is weak it has a clear signature through the angular dependence of the absorption process. Based on recent studies on oriented single crystals [22,24–27] we estimate that quadrupole-allowed peaks will be at most 1% in powder samples which is considerably smaller than the A_i peaks observed for the substituted manganites but perhaps not negligible. A small quadrupole component, as seen for example in FeO, [27] may well be present.

- *Dipole allowed via 3d-4p mixing on the absorbing atom*
  If the Mn site lacks inversion symmetry, then in principle there will be mixing of the Mn 3d and 4p states on the central atom. Consider a system that is nearly cubic but has a small distortion that removes the inversion symmetry - i.e. the metal atom is slightly displaced such that the bonds on opposite sides of the metal atom are slightly different. Then the mixing parameter is $\sim \delta_l/r_o$ and the matrix element will be proportional to $(\delta_l/r_o)^2$, where δ_l is the difference in opposite bond lengths and r_o is the average bond length. An example is the V site in V_2O_5; here the VO_6 octahedron

is strongly distorted, [25,26] and along the c-axis, the two V-O bond lengths are 1.577 and 2.791 Å respectively. Experimentally there is a large pre-edge peak for the V K-edge that can be modeled assuming 3d-4p mixing on the absorbing atom plus the effect of a corehole.

- *Dipole allowed via 4p mixing with neighboring metal atom 3d states*
  In several cases, a significant pre-edge peak is observed in a cubic crystal, which can't be explained by the above 3d-4p mixing on the excited atom. Multi-scattering calculations for such systems often show that large clusters are needed before the pre-edge features are produced - scattering paths are needed which include many further neighbors, particularly the second neighbor metal atoms. An equivalent result emerges from band theory calculations where the hybridization of extended states is important. Here the dipole transition can be made allowed via mixing of the 4p state on the central atom with the 3d states on neighboring atoms. Projections of the density of states with p character (p-DOS) for such systems show small features at the energies of the 3d states; such features are not observed in the p-DOS when the pre-edge feature is a quadrupole transition. In the limit of multi-scattering calculations with very large clusters, the two approaches (band theory and multi-scattering) should be equivalent.

To have a mixing of 3d with the 4p states (to make a state of p-character), one needs a combination of 3d states that has odd parity as pointed out by Elfimov *et al.* [36]. It is easy to obtain such a state if a linear combination of 3d states on two neighboring Mn atoms is used and the p-states are extended enough to partially overlap them. Specifically, consider 3 Mn atoms in a line - a central excited atom (0) and left (L) and right (R) atoms - with $\Psi_{4p}(0)$ being the 4p state on the central atom, and $\Psi_{3d;x^2-y^2}(\mathrm{R}_R)$ and $\Psi_{3d;x^2-y^2}(\mathrm{R}_L)$ being the $3\mathrm{d}_{x^2-y^2}$ states centered on the right and left atoms. Then a state with odd symmetry about the central atom is given by

$$\Psi_{total} = \alpha\Psi_{4p}(0) + \frac{\beta}{\sqrt{2}}(\Psi_{3d;x^2-y^2}(R_L) - \Psi_{3d;x^2-y^2}(R_R)) \tag{2}$$

where α is essentially 1.0 and we ignore the intervening O atom via which the hybridization occurs. The small parameter, β, is a measure of the hybridization and is strongly dependent on the overlap of the 4p and 3d wavefunctions on different Mn atoms, and hence on the distance between them.

2. Application to the substituted manganites

The pre-edge for the substituted manganites follows the general trends observed for other Mn systems quite well. Three A-peaks are observed for $CaMnO_3$; A_2 is larger than the A_1 peak, and the A_2-A_1 splitting is smaller (high valence - +4) than for other samples. The $LaMnO_3$ case is similar; the A_2-A_1 splitting is largest (lower valence +3) and the overall A peak amplitude is smallest. However, the A_2 peak is larger than expected from the literature for Mn^{+3} states in other compounds [23], possibly because of increased local distortions in this compound.

However, there are difficulties with some of the earlier interpretations [28,23] in which the dipole allowed transitions are assumed to originate from a 3d-4p mixing on the excited atom. First the A_i peaks appear for both distorted and undistorted systems. Second, the amplitude (particularly for the relatively undistorted system $CaMnO_3$) is too large to be a 1s-3d transition made allowed by a slight breaking of inversion symmetry about the excited Mn atom. Recently, based on the calculations of Elfimov *et al.* [36], we have interpreted A_1 and A_2 as dipole allowed via a mixing of Mn 4p states with Mn 3d states on neighboring metal atoms [46]. The projected p-DOS in the calculations of Elfimov *et al.* [36] show two features in the pre-edge region, which indicates that dipole-allowed transitions should be present. In addition, the broad Mn 4p band obtained in that work and by by Benfatto *et al.* [47], also implies that the 4p states are indeed extended - a necessary requirement for mixing with the 3d states on the neighboring metal atoms. Similar interpretations have been given recently for other transition metal systems that are cubic or very nearly so; Fe in FeO [27] and Ti in rutile [22,24]. A mixing with the 3d states on neighboring Ti atoms was also reported in the layered disulfide TiS_2 [51].

The calculations of Elfimov *et al.* also show that there is a splitting of the unfilled 3d bands - the lowest is the majority e_g band (which may be partially filled via doping); the next two are the minority e_g and t_{2g} bands which partially overlap. The coupling with the t_{2g} is expected to be smaller since these orbitals are of the form d_{xy}, which has reduced overlap with the Mn 4p in a π bonding configuration. The splitting of these e_g bands depends both on J_H and on the degree of covalency/hybridization. As reported recently, [46] adjusting the parameters in this calculation so that the theoretical splitting is close to the 2 eV observed experimentally, resulted in U=4 eV and J_H=0.7 eV. These lower values also suggest an increase in covalency and hence that the charge is shared between Mn and O. Consequently, there is a non-zero density of holes in the O bands, in agreement with Ju *et al.* [35] and these O-holes may play an important role in the unusual transport of these materials. For the CMR samples, the additional decrease in the A_1-A_2 splitting for $T<T_c$ may suggest a further increase in covalency.

Finally the temperature dependence of the A_i peak amplitudes is still not explained. Comparing the pre-edges of distorted $LaMnO_3$ [46] with almost undistorted $CaMnO_3$ (See Fig. 5) would suggest that as the CMR samples change from distorted above T_c to ordered at low T, the A_2 peak would increase relative to A_1. Experimentally the reverse is true. However, we still suggest that the observed temperature dependence arises from the change in local structure, based on the fact that the changes for the CMR and CO samples are out of phase for both the pre-edge features and the structure in the main edge.

3. Other Models

Another general feature that emerges from our data is that although the main changes occur just below T_c, there is also a gradual change to the fully ordered state as the sample is cooled well below T_c, and the local structure continues to change down to 50K and below. Consequently there may be clusters formed at T_c that grow as T is lowered. We have interpreted our local distortion results earlier in terms of a two component model. [14] Within that model, one of these components (fluids) would correspond to delocalized states

- these could be either delocalized holes or delocalized electrons. We also point out that the decreasing distortions observed in EXAFS as T is decreased below T_c and the corresponding increase in resistivity suggest a changing average mobility of the charge carriers. Within the model we have suggested, the fraction of delocalized carriers would increase as T is lowered. [15] However, one of these components might also correspond to the Mn atoms in a cluster, the positions of which are dominated by small variations in dopant concentration or O vacancies, possibly leading to a regime with phase separation. Such inhomogeneities likely play an import role in these materials. In addition, Jaime *et al.* [52] have successfully modeled their resistivity and thermoelectric measurements using a two component system of localized and itinerant carriers. The recent calculations using the Kondo model [53–55] also stress phase separation but it is not clear how to compare with their results.

V. CONCLUSIONS

We have addressed several issues related to the Mn valence in the substituted $LaMnO_3$ materials. Although discussions of these systems often assume isolated Mn^{+3} and Mn^{+4} states, we observe no change (< 0.02 eV) in the average edge position through the ferromagnetic transition for the CMR systems (Ca, Ba or Pb doped), and in all cases the total edge shift from 0 to 300K is < 0.04 eV. Although there is no obvious step or kink in the edge, expected for two well-defined valence states, there is a very small shape change that can be observed by taking the difference of data files at different temperatures. A dip/peak structure develops as T drops below T_c for the CMR samples; the dip/peak separation is ~ 2 eV and is consistent with the splitting calculated [36] for the p_x and p_y partial DOS when the manganite structure changes from an undistorted to a distorted ($LaMnO_3$) lattice. For CMR samples, such changes in the local distortions below T_c were deduced earlier from EXAFS data [13–16]. At low T the CMR samples are very well ordered, but as T increases there is a rapid increase in the local distortions up to $T=T_c$; above T_c the change in disorder changes slowly. The rapid change just below T_c has been associated with the formation of polarons. These distortions, now observed in both the XANES and EXAFS data, indicate some change in the local charge distribution. However the small size of the effect in the XANES spectra needs to be understood. In part it can be attributed to the extended nature of the broad Mn 4p band which tends to make the 1s-4p edge transition an average over several Mn atoms. However a change in covalency - specifically a transfer of charge between Mn 3d and O 2p states - might also be associated with this structural change, but produce little change in the edge. Support for this possibility is obtained from the pre-edge results, summarized below.

For the CO sample we observe a similar behavior, but in this case the structure in the difference spectra are inverted relative to that for the CMR sample. This indicates that the local distortions increase in the CO state below T_{CO}.

The pre-edge structure provides additional information about the 3d-bands in these materials. Two or three peaks are observed, labeled A_1-A_3. A_2 at 300K is essentially independent of concentration while A_1 increases slowly with x; A_3 is only observed for high Ca concentrations. Following the work of Elfimov *et al.* [36] we attribute these peaks to a hybridization of Mn 4p on the excited atom with an ungerade combination of 3d states

on neighboring Mn atoms, i.e. they are not the result of splittings of atomic multiplets on the excited atom as is often assumed. Similar explanations for the pre-edge region have recently been proposed for several other transition metal K-edges. Consequently the splittings observed are essentially unaffected by the presence of the core hole and should be a good measure of the splittings of the e_g bands which are influenced by the hybridization of the Mn 3d and O 2p states. This interpretation of the pre-edge does not depend on small distortions of the crystal and therefore also provides a simple explanation for the large pre-edge features observed in the more ordered $CaMnO_3$ material.

In the calculations of Elfimov*et al.* [36], the two lowest empty bands are the majority and minority spin e_g bands; the minority spin t_{2g} band overlaps the latter but is expected to be more weakly coupled. U and J must be reduced slightly to fit the experimental splitting (2 eV) of the A_1 and A_2 peaks; U=4eV and J_H=0.7eV. This indicates an increase in the covalency. The additional small decrease in the A_1-A_2 splitting below T_c may suggest a further change in covalency or hybridization.

Thus the picture that emerges is that there is considerable hybridization of the energy states (Mn 4p and 3d, and O 2p), with some hole density in the O bands and possibly only small differences in the charge localized on Mn atoms which have different types of e_g orbitals. The possibility of distinct types of orbitals can lead to orbital ordering [19], with displacements of the O atoms forming J-T-like Mn-O bond distortions when the hopping charge is localized for times of order the optical phonon periods. As a result, the possibility that part of the transport takes place via hole density in the O bands needs to be considered. Note that slowly hopping holes on the O sites would lead to distorted Mn-O bonds while rapid hopping (faster than phonons) would leave the O atom at an average undistorted position.

ACKNOWLEDGMENTS

The authors wish to thank G. Brown, C. Brouder, D. Dessau, T. Geballe, J. Rehr, G. Sawatzky, and T. Tyson for useful discussions and comments. FB thanks K. Terakura for sending some of their unpublished results. The experiments were performed at the Stanford Synchrotron Radiation Laboratory, which is operated by the U.S. Department of Energy, Division of Chemical Sciences, and by the NIH, Biomedical Resource Technology Program, Division of Research Resources. Some experiments were carried out on UC/National Laboratories PRT beam time. The work is supported in part by NSF grant DMR-97-05117.

REFERENCES

[1] J. Volger, Physica (Amsterdam) **20**, 49 (1954).
[2] E. O. Wollan and W. C. Koehler, Phys. Rev. **100**, 545 (1955).
[3] P. Schiffer, A. Ramirez, W. Bao, and S-W. Cheong, Phys. Rev. Lett. **75**, 3336 (1995).
[4] G. H. Jonker and J. H. van Santen, Physica (Amsterdam) **16**, 337 (1950).
[5] A. P. Ramirez, P. Schiffer, S-W. Cheong, C. H. Chen, W. Bao, T. T. M. Palstra, P. L. Gammel, D. J. Bishop, and B. Zegarski, Phys. Rev. Lett. **76**, 3188 (1996).
[6] C. H. Chen, S-W. Cheong, and H. Y. Hwang, J. Appl. Phys. **81**, 4326 (1997).
[7] C. Zener, Phys. Rev. **82**, 403 (1951).
[8] P. W. Anderson and H. Hasegawa, Phys. Rev. **100**, 675 (1955).
[9] P. G. de Gennes, Phys. Rev. **118**, 141 (1960).
[10] A. J. Millis, P. B. Littlewood, and B. I. Shraiman, Phys. Rev. Lett. **74**, 5144 (1995).
[11] A. J. Millis, B. I. Shraiman, and R. Mueller, Phys. Rev. Lett. **77**, 175 (1996).
[12] H. Röder, J. Zang, and A. R. Bishop, Phys. Rev. Lett. **76**, 1356 (1996).
[13] C. H. Booth, F. Bridges, J. Boyce, T. Claeson, B. M. Lairson, R. Liang, and D. A. Bonn, Phys. Rev. B **54**, 9542 (1996).
[14] C. H. Booth, F. Bridges, G. H. Kwei, J. M. Lawrence, A. L. Cornelius, and J. J. Neumeier, Phys. Rev. Lett. **80**, 853 (1998).
[15] C. H. Booth, F. Bridges, G. H. Kwei, J. M. Lawrence, A. L. Cornelius, and J. J. Neumeier, Phys. Rev. B **57**, 10440 (1998).
[16] G. Subías, J. García, M. G. Proietti, and J. Blasco, Phys. Rev. B **56**, 8183 (1997).
[17] S. J. L. Billinge, R. G. DiFrancesco, G. H. Kwei, J. J. Neumeier, and J. D. Thompson, Phys. Rev. Lett. **77**, 715 (1996).
[18] N. Nücker, J. Fink, J. C. Fuggle, and P. J. Temmerman, Phys. Rev. B **37**, 5158 (1988).
[19] V. L. Anisimov, I. S. E. amd M. A. Korotin, and K. Terakura, Phys. Rev. B **55**, 15494 (1997).
[20] T. Mizokawa and A. Fujimori, Phys. Rev. B **56**, R493 (1997).
[21] T. A. Tyson, Q. Qian, C.-C. K. J.-P. Rueff, F. M. F. deGroot, M. Croft, S.-W. Cheong, M. Greenblatt, and M. A. Subramanian, Phys. Rev. B **60**, 4665 (2000).
[22] Y. Joly, D. Cabaret, H. Renevier, and C. R. Natoli, Phys. Rev. Lett. **82**, 2398 (1999).
[23] A. Manceau, A. I. Gorshkov, and V. A. Drits, Amer. Mineral. **77**, 1133 (1992).
[24] Y. Aïfa, B. Poumellec, V. Jeanne-Rose, R. Cortes, R. V. Vedrinskii, and V. L. Kraizman, J. Phys. IV **7**, C2 (1997).
[25] B. Poumellec, V. Kraizman, Y. Aifa, R. Cortès, A. Novakovich, and R. Vedrinskii, Phys. Rev. B **58**, 6133 (1998).
[26] O. Sipr, A. Simunek, S. Bocharov, T. Kirchner, and G. Dräger, Phys. Rev. B **60**, 14115 (1999).
[27] D. Heumann, G. Dräger, and S. Bocharov, J. Phys. IV **7**, C2 (1997).
[28] M. Belli, A. Scafati, A. Bianconi, S. Mobilio, L. Pallandino, A. Reale, and E. Burattini, Solid State Commun. **35**, 355 (1980).
[29] S. Satpathy, Z. S. Popović, and F. R. Vukajlović, Phys. Rev. Lett. **76**, 960 (1996).
[30] W. E. Pickett and D. J. Singh, Phys. Rev. B **53**, 1146 (1996).
[31] P. Dai, J. D. Zhang, H. A. Mook, S.-H. Liou, P. A. Dowben, and E. W. Plummer, Phys. Rev. B **54**, 3694 (1996).

[32] G. Zhao, K. Conder, H. Keller, and K. A. Müller, Nature **381**, 676 (1996).
[33] J.-S. Zhou, J. B. Goodenough, A. Asamitsu, and Y. Tokura, Phys. Rev. Lett. **79**, 3234 (1997).
[34] G. H. Kwei, D. N. Argyriou, S. J. L. Billinge, A. C. Lawson, J. J. Neumeier, A. P. Ramirez, M. A. Subramanian, and J. D. Thompson, in *Epitaxial Oxide Thin Films III*, MRS Symposia Proceedings (Materials Research Society, Pittsburgh, 1997), No. 475, p. 533.
[35] H. L. Ju, H.-C. Sohn, and K. M. Krishman, Phys. Rev. Lett. **79**, 3230 (1997).
[36] I. S. Elfimov, V. I. Anisimov, and G. A. Sawatzky, Phys. Rev. Lett. **82**, 4264 (1999).
[37] G. J. Snyder, R. Hiskes, S. DiCarolis, M. R. Beasley, and T. H. Geballe, Phys. Rev. B **53**, 14434 (1996).
[38] J. Mitchell, J. E. Millburn, M. Medarde, S. Short, and J. D. Jorgensen, J Solid State Chem. **141**, 599 (1998).
[39] M. E. Leonowicz, K. R. Poeppelmeier, and J. Longo, J. Solid State Chem. **59**, 71 (1985).
[40] G. Subías, J. García, J. Blasco, and M. G. Proietti, Phys. Rev. B **57**, 748 (1998).
[41] I. Maurin, P. Barboux, Y. Laissailly, J. P. Boilot, and F. Villain (unpublished).
[42] R. S. Liu, L. Y. Jang, J. M. Chen, Y. C. Tsai, Y. D. Hwang, and R. G. Liu, J Solid State Chem **128**, 326 (1994).
[43] H. Yamaguchi, A. Yamada, and H. Uwe, Phys. Rev. B **58**, 8 (1998).
[44] M. Croft, D. Sills, M. Greenblatt, C. Lee, S.-W. Cheong, K. V. Ramanujachary, and D. Tran, Phys. Rev. B **55**, 8726 (1997).
[45] T. Ressler and J. W. *et al.* (unpublished).
[46] F. Bridges, C. H. Booth, G. H. Kwei, J. Neumeier, and G. A. Sawatzky, Phys. Rev. B **61**, R9237 (2000).
[47] M. Benfatto, Y. Joly, and C. R. Natoli, Phys. Rev. Lett. **83**, 636 (1999).
[48] A. Bianconi, in *X-ray Absorption: principles, applications, techniques of EXAFS, SEXAFS and XANES*, edited by D. C. Koningsberger and R. Prins (John Wiley and Sons, New York, 1988), p. 594.
[49] J. S. Griffith, in *THe Theory of Transition Metal Ions* (Cambridge University Press, Cambridge, 1961).
[50] S. Sugano, Y. Tanabe, and H. Kamimura, in *Multiplets of Transition-Metal Ions* (Academic Press, New York, 1970).
[51] Z. Y. Wu, G. Ouvrard, P. Moreau, and C. R. Natoli, Appl. Phys. Lettev. B **55**, 9508 (1997).
[52] M. Jaime, P. Lin, S. H. Chun, M. B. Salamon, P. Dorsey, and M. Rubinstein, Phys. Rev. B **60**, 1028 (1999).
[53] S. Yunoki, J. Hu, A. L. Malvezzi, A. Moreno, N. Furukawa, and E. Dagotto, Phys. Rev. Lett. **80**, 845 (1998).
[54] S. Yunoki and A. Moreno, Phys. Rev. B **58**, 6403 (1998).
[55] E. Dagotto, S. Yunoki, A. L. Malvezzi, A. Moreno, and H. Ju, Phys. Rev. B **58**, 6414 (1998).

FIGURES

FIG. 1. The Mn K-edges for a number of similar manganite systems, corrected for energy shifts of the monochromator (see text).

FIG. 2. Fits of absorption edges to each other. In a) and b) we show fits of the $LaMnO_3$ edge (solid curve) to the 25% and 100% Ca samples. In c) and d) we show fits of the 50K data (solid curve) to high temperature data for two different samples. Corrections from the reference Mn foil have not been included in this figure.

FIG. 3. The shift of the Mn K-edge with a) Ca concentration and b) titrated valence for $La_{1-x}Ca_xMnO_3$. Note we do not have titration data for x=0.30. The relative errors are: edge shift, $\pm$ 0.02 eV, smaller than symbols; Mn valence $\pm$ 0.02 units, slightly larger than symbols. In this and several following figures, the lines are a guide to the eye only.

FIG. 4. The shift of the absorption edge for each sample relative to the low temperature data. In panels a)-c), one of the curves (squares) is shifted downward by 0.1 eV for clarity. Relative errors $\pm$ 0.015 eV; $\pm$ 0.03 eV for $LaMnO_{3.03}$.

FIG. 5. The temperature dependence of the pre-edge region for $CaMnO_3$, 21% Ca, and 33% Ba; note different temperature ranges. The $CaMnO_3$ sample shows little change of the pre-edge region below 300K while the A_1 and A_2 peaks are temperature dependent for the CMR samples. The Ba pre-edge data, collected using Si(220), are much sharper than data collected using Si(111) crystals, and show a splitting of the A peak. Note that the data collected using Si(220) in c) have been shifted down by 0.15 eV for clarity.

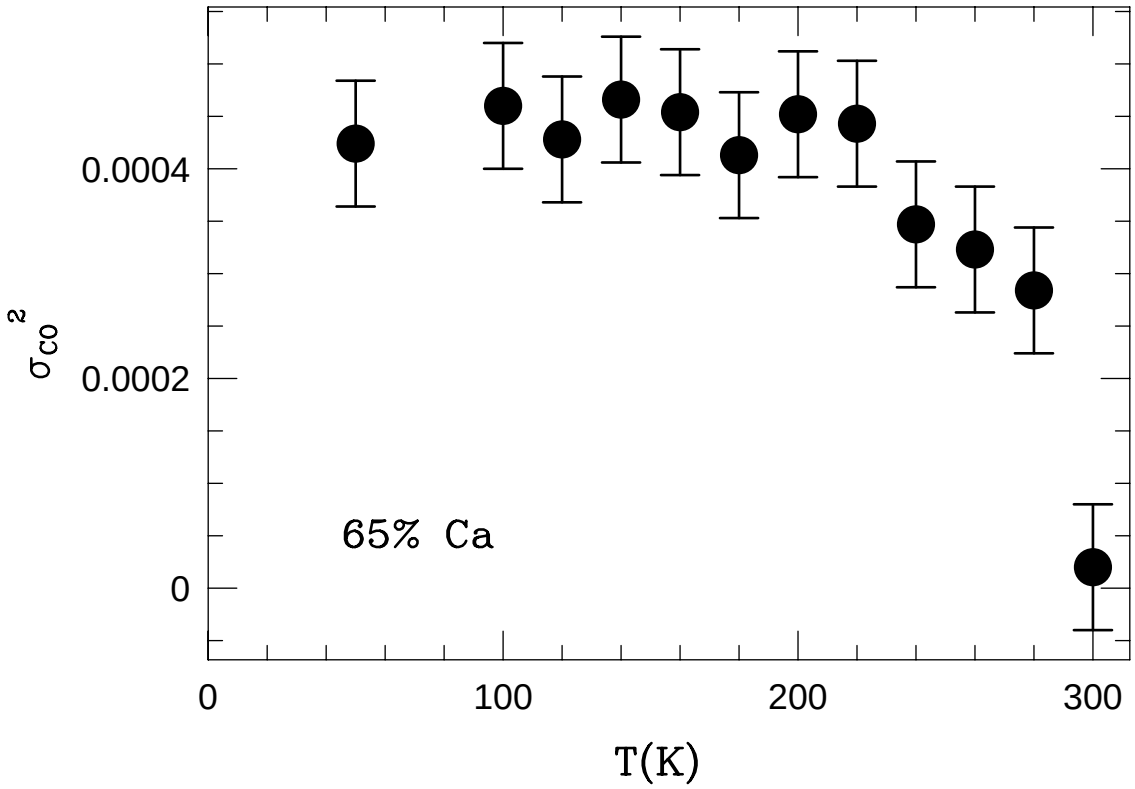
FIG. 6. The temperature dependence of the pre-edge region for $La_{0.7}Ca_{0.3}MnO_3$, $Sr_3Mn_2O_{6.55}$ and the 33% Pb samples up to roughly 300K. The leading edge of the A_1 peak is broader for $Sr_3Mn_2O_{6.55}$ than for the 30% Ca sample in a). In b) the Pb samples has the largest A_1 peak at low T. Note that the scale is expanded compared to the previous figures and the B peak is not shown.

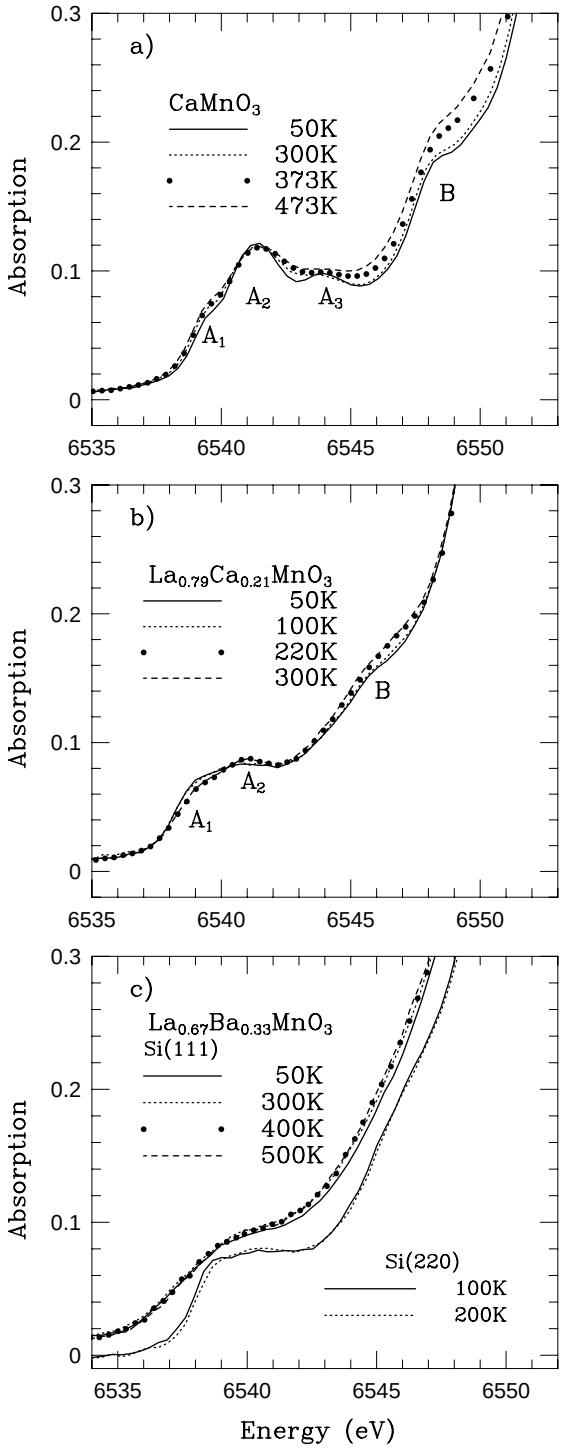
FIG. 7. The positions of the pre-edge features as a function of Ca concentration - open symbols, and solid circles, 300K. The error in peak position is $\pm$ 0.1 eV. For the CMR samples, the A_2 peak is shifted to a lower energy for $T < T_c$ - the filled triangles are for 50K.

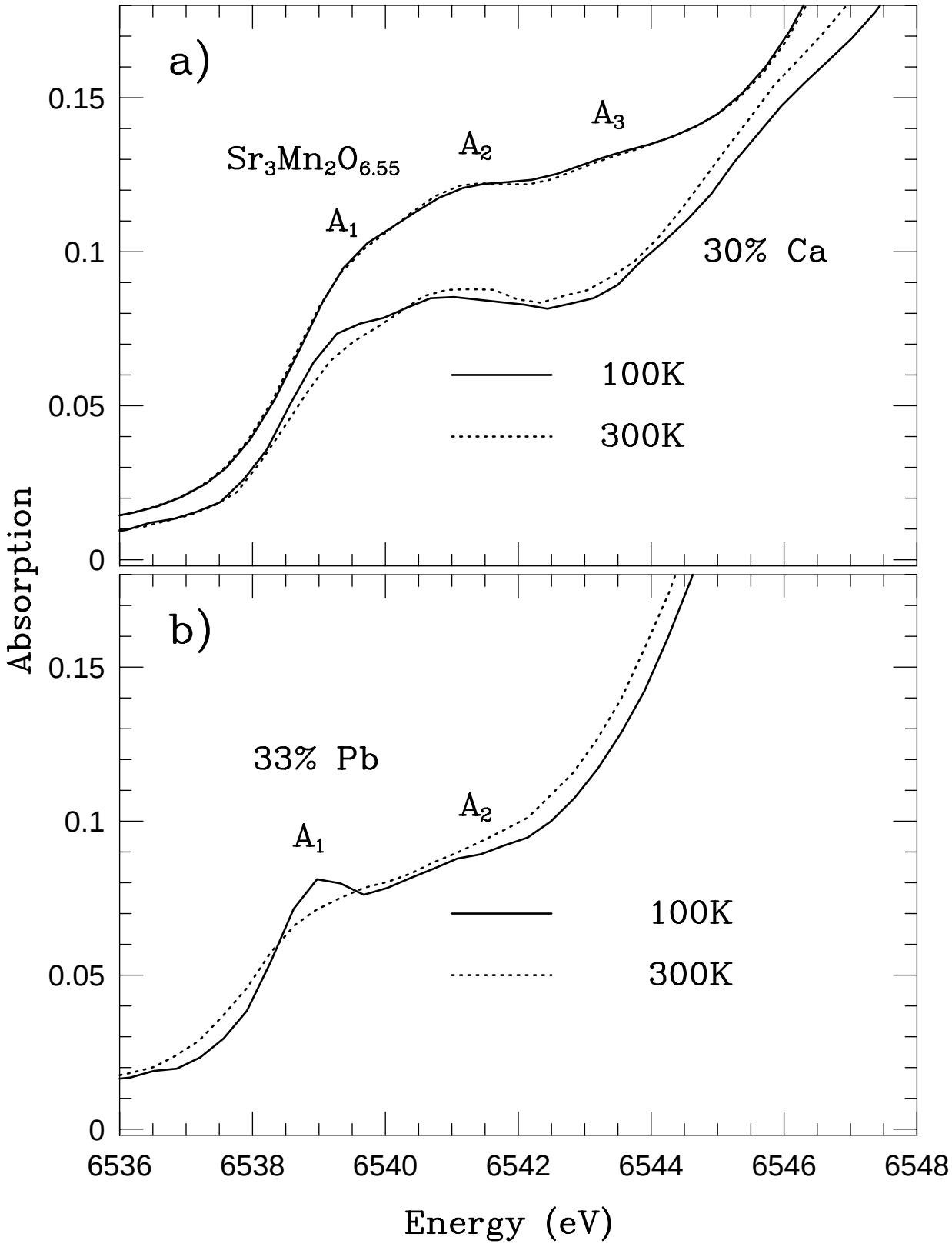
FIG. 8. The difference spectra as a function of temperature for 21, 30 and 65% Ca, and the end compounds. The main edge is included above each set of traces (multiplied by 0.03 to fit on the graph) to show where the structure is located relative to the edge. Note the inversion of the structure for the CO sample (T_{CO} = 270K) (b), compared to the CMR samples (c) (21% Ca, T_c $\sim$ 210K) and d) (30% Ca, $T_c \sim$ 260K).

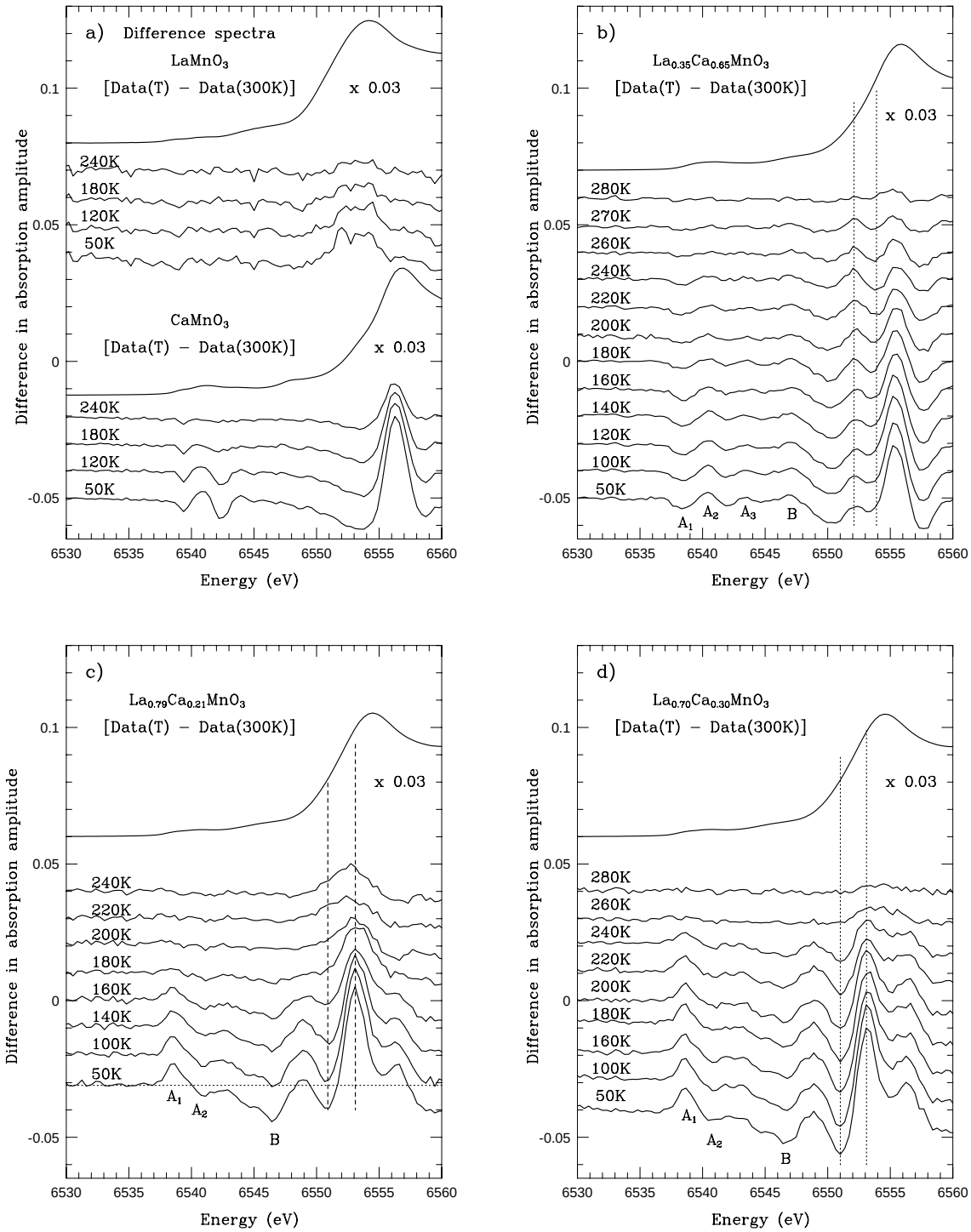
FIG. 9. A comparison of the data for the 65% Ca sample and a simulation obtained from a 35-65% weighted sum of the $LaMnO_3$ and $CaMnO_3$ end compounds. The experimental edge is significantly sharper.

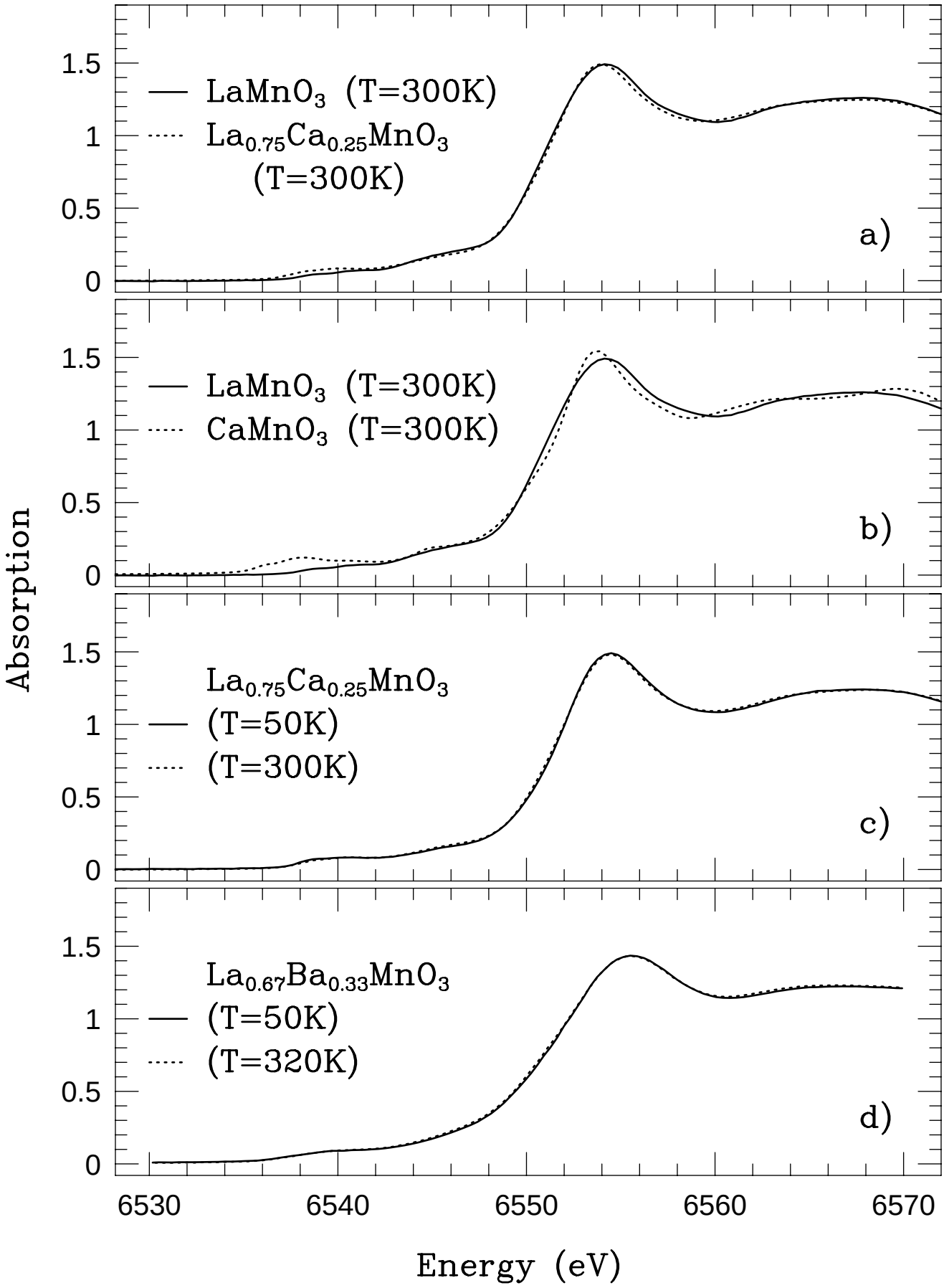
FIG. 10. A plot of $\sigma^2_{CO}(T)$ for the Mn-O bond as a function of T (65% Ca sample). $\sigma^2_{CO}(T)$ is extracted from the σ^2_{Mn-O}(T) data presented in Ref. [15]. $T_{CO} \sim$ 270K.

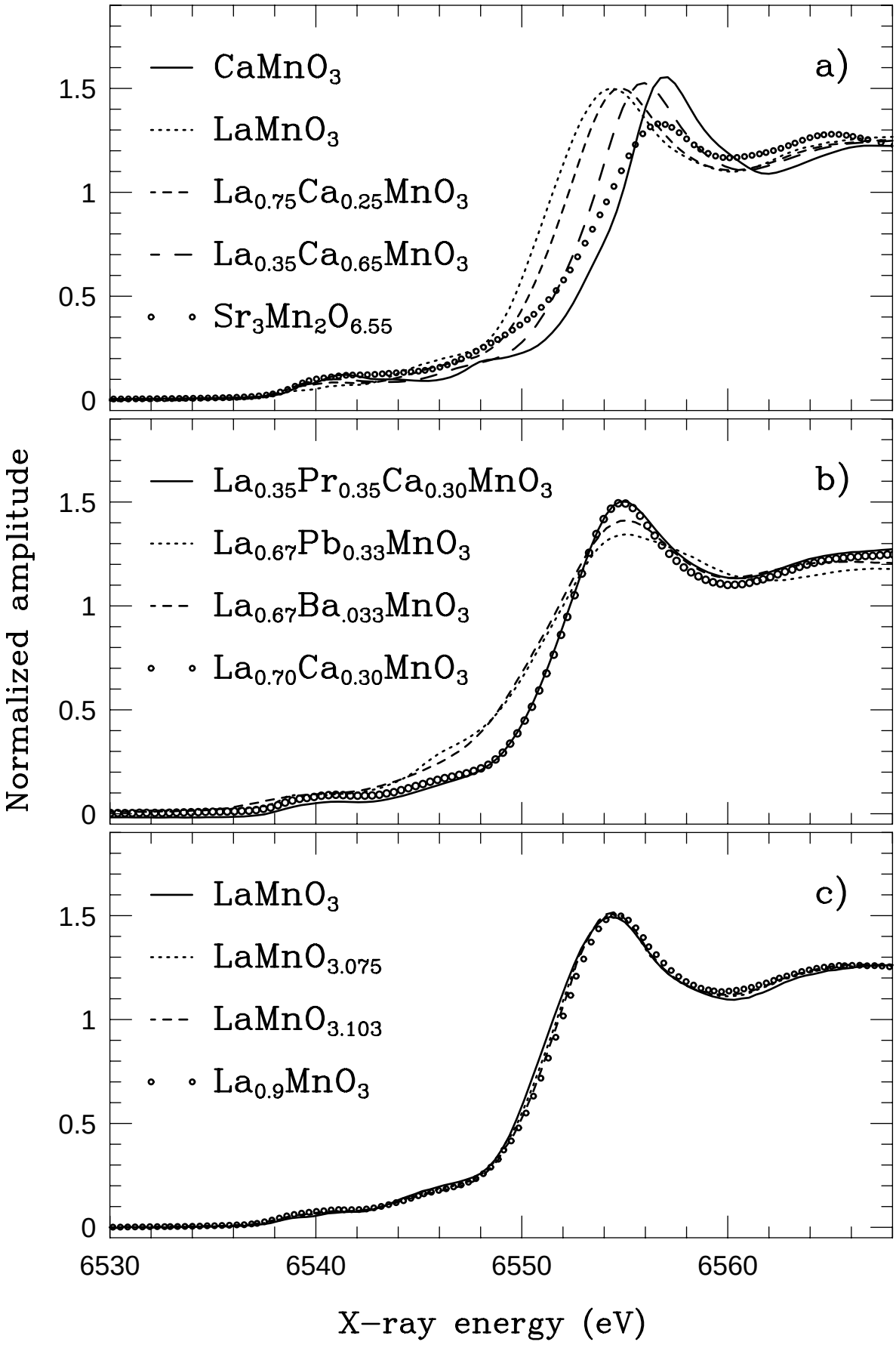

0.0004
0.0002
0
σ_{co}^2
65% Ca
0
100
200
300
T(K)

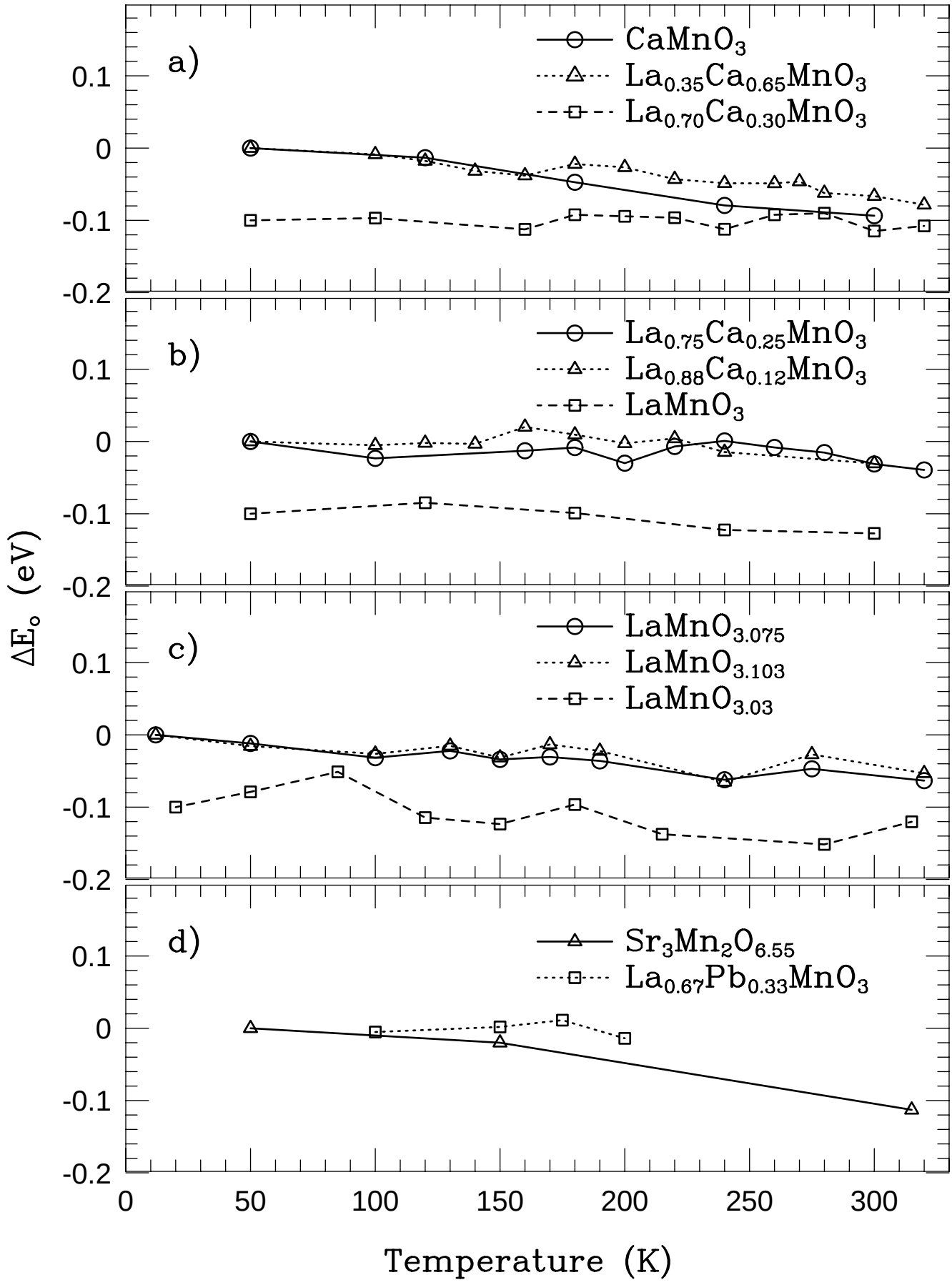

a)
$CaMnO_3$
50K
300K
373K
473K
A_1
A_2
A_3
B
b)
$La_{0.79}Ca_{0.21}MnO_3$
50K
100K
220K
300K
A_1
A_2
B
c)
$La_{0.67}Ba_{0.33}MnO_3$
Si(111)
50K
300K
400K
500K
Si(220)
100K
200K
Absorption
Energy (eV)
0
0.1
0.2
0.3
6535
6540
6545
6550

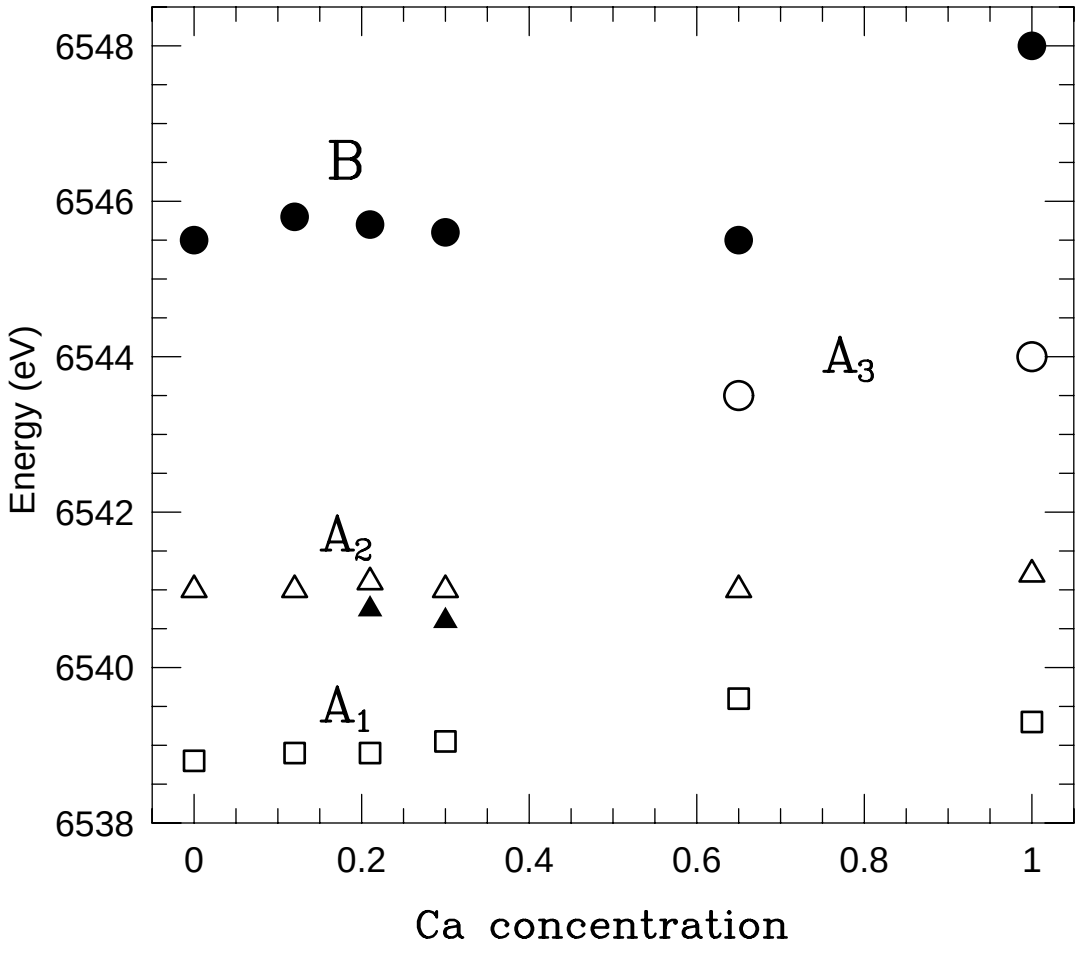

a)
$Sr_3Mn_2O_{6.55}$
A_1
A_2
A_3
30% Ca
100K
300K
b)
33% Pb
A_1
A_2
100K
300K
Absorption
Energy (eV)
0
0.05
0.1
0.15
6536
6538
6540
6542
6544
6546
6548

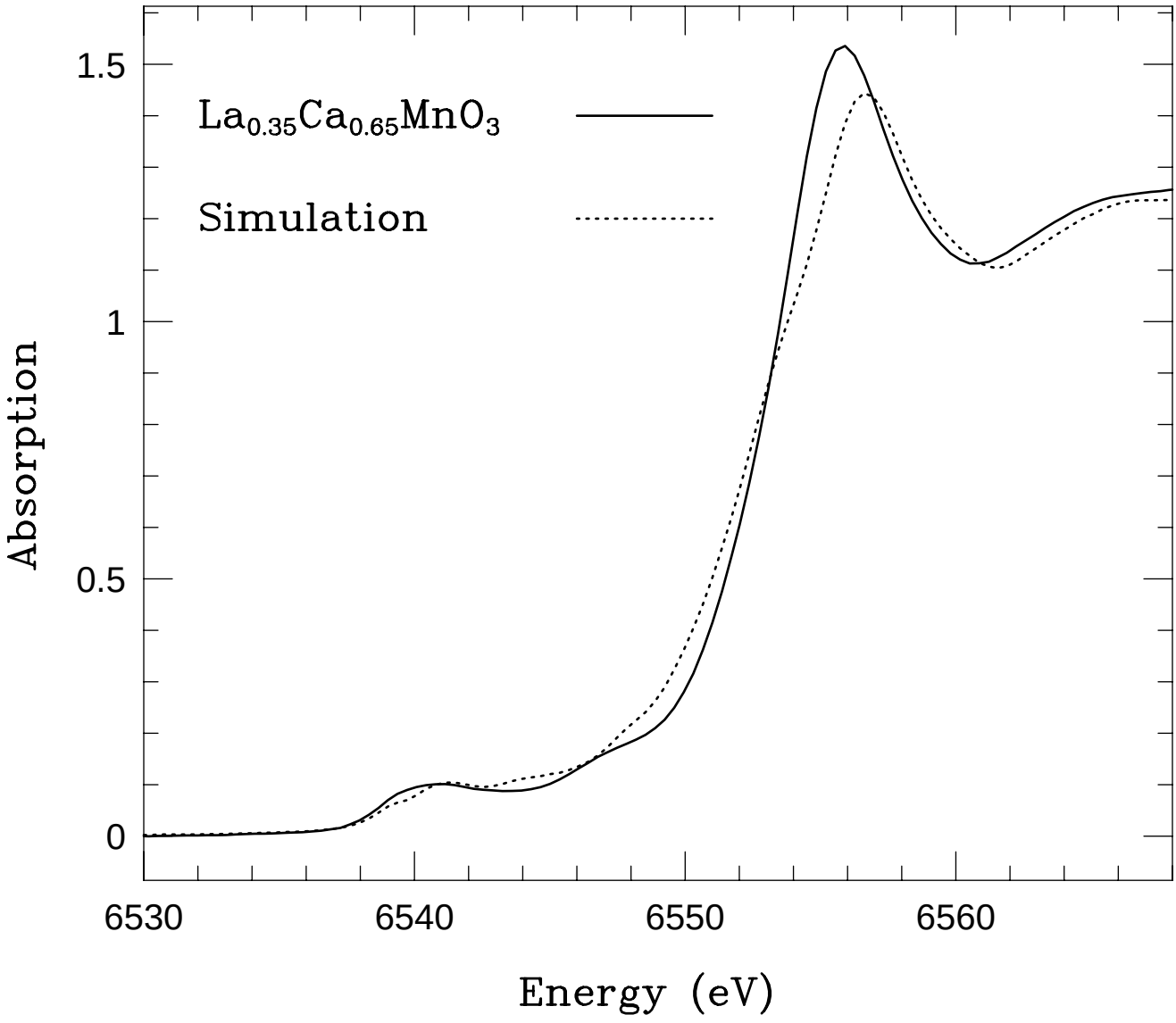

a) Difference spectra
LaMnO3
[Data(T) − Data(300K)]
x 0.03
240K
180K
120K
50K
CaMnO3
[Data(T) − Data(300K)]
x 0.03
240K
180K
120K
50K
Difference in absorption amplitude
Energy (eV)
b)
La0.35Ca0.65MnO3
[Data(T) − Data(300K)]
x 0.03
280K
270K
260K
240K
220K
200K
180K
160K
140K
120K
100K
50K
A1
A2
A3
B
Difference in absorption amplitude
Energy (eV)
c)
La0.79Ca0.21MnO3
[Data(T) − Data(300K)]
x 0.03
240K
220K
200K
180K
160K
140K
100K
50K
A1
A2
B
Difference in absorption amplitude
Energy (eV)
d)
La0.70Ca0.30MnO3
[Data(T) − Data(300K)]
x 0.03
280K
260K
240K
220K
200K
180K
160K
100K
50K
A1
A2
B
Difference in absorption amplitude
Energy (eV)

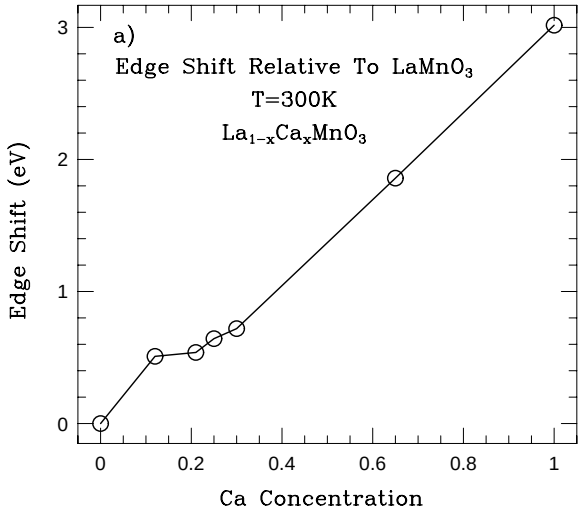

LaMnO3 (T=300K)
La0.75Ca0.25MnO3 (T=300K)
a)
LaMnO3 (T=300K)
CaMnO3 (T=300K)
b)
La0.75Ca0.25MnO3
(T=50K)
(T=300K)
c)
La0.67Ba0.33MnO3
(T=50K)
(T=320K)
d)
Absorption
Energy (eV)
0
0.5
1
1.5
6530
6540
6550
6560
6570

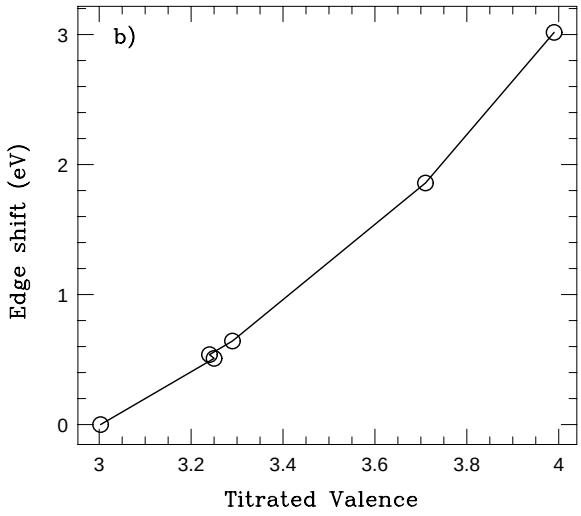

CaMnO3
LaMnO3
La0.75Ca0.25MnO3
La0.35Ca0.65MnO3
Sr3Mn2O6.55
a)
La0.35Pr0.35Ca0.30MnO3
La0.67Pb0.33MnO3
La0.67Ba.033MnO3
La0.70Ca0.30MnO3
b)
LaMnO3
LaMnO3.075
LaMnO3.103
La0.9MnO3
c)
Normalized amplitude
X−ray energy (eV)
0
0.5
1
1.5
6530
6540
6550
6560


a)
$CaMnO_3$
$La_{0.35}Ca_{0.65}MnO_3$
$La_{0.70}Ca_{0.30}MnO_3$
b)
$La_{0.75}Ca_{0.25}MnO_3$
$La_{0.88}Ca_{0.12}MnO_3$
$LaMnO_3$
c)
$LaMnO_{3.075}$
$LaMnO_{3.103}$
$LaMnO_{3.03}$
d)
$Sr_3Mn_2O_{6.55}$
$La_{0.67}Pb_{0.33}MnO_3$
ΔE_o (eV)
0.1
0
-0.1
-0.2
0
50
100
150
200
250
300
Temperature (K)


6548
6546
6544
6542
6540
6538
Energy (eV)
B
A3
A2
A1
0
0.2
0.4
0.6
0.8
1
Ca concentration


La0.35Ca0.65MnO3
Simulation
Absorption
Energy (eV)
0
0.5
1
1.5
6530
6540
6550
6560


a)
Edge Shift Relative To $LaMnO_3$
T=300K
$La_{1-x}Ca_xMnO_3$
Edge Shift (eV)
Ca Concentration
0
1
2
3
0
0.2
0.4
0.6
0.8
1


b)
Edge shift (eV)
Titrated Valence
0
1
2
3
3
3.2
3.4
3.6
3.8
4